Journal of Membrane Science 364 (2010) 17–26

Contents lists available at ScienceDirect

Journal of Membrane Science

journal homepage: www.elsevier.com/locate/memsci

Dry reforming of methane in membrane reactors using Pd and Pd–Ag composite membranes on a NaA zeolite modified porous stainless steel support

M.L. Bosko, J.F. Múnera, E.A. Lombardo, L.M. Cornaglia*

Instituto de Investigaciones en Catálisis y Petroquímica (FIQ, UNL-CONICET), Santiago del Estero 2829, 3000 Santa Fe, Argentina

ARTICLE INFO

Article history:
Received 27 May 2010
Received in revised form 20 July 2010
Accepted 22 July 2010
Available online 11 August 2010

Keywords:
Membrane reactor
Methane dry reforming
NaA zeolite

ABSTRACT

This paper reports the results obtained with different composite membranes used on a membrane reactor for the production of high purity hydrogen. The dry reforming of methane was carried out over a Rh/La_2O_3 catalyst. Two types of composite membranes were synthesized, Pd and a Pd–Ag alloy. The metal films were deposited by electroless plating on modified porous stainless steel. The support surface was previously modified with a NaA zeolite by dip coating and hydrothermal synthesis. The composition and crystalline structures of the alloy films were characterized by scanning electron microscopy (SEM), energy-dispersive X-ray analysis (EDS), X-ray diffraction (XRD) and X-ray photoelectron spectroscopy (XPS). The membrane reactor was designed and built to use either the Pd or the Pd–Ag composite membrane whose crystalline structure and typical morphology were not affected after different reaction conditions. The Pd membrane showed the best behavior in the membrane reactor with the highest methane conversion, H_2/CH_4 selectivity and permeation flux. After operation of the membranes at 450–500 °C on stream for up to 570 h no modification of the permeation parameters was observed.

© 2010 Elsevier B.V. All rights reserved.

1. Introduction

The driving forces for the use of H_2 as an energy carrier are energy independence and environmental protection [1]. H_2 can be produced from a large variety of widely available raw materials such as fossil fuels, coal, biomass and alcohols, natural gas being today the main source worldwide. The main limitation to the widespread use of H_2 as a fuel for PEM fuel cells is the cost of production and purification. Therefore, it is not surprising that membrane reactors (MRs) could be considered an economical option because they produce pure H_2 in a single vessel, thus eliminating or greatly simplifying the purification steps needed to comply with the purity requirements of PEM FC.

The use of MRs for methane dry reforming has been explored employing several types of membranes and catalysts [2–4]. Lee et al. [5] studied the effect of pressure in a membrane reactor equipped with silica-based membranes. They found that the yield of hydrogen in the MR at first rose with pressure because of increasing permeability, but then dropped because of the unfavorable equilibrium and enhanced rate of the reverse reaction. Their studies were conducted at non-equilibrium conditions.

Our group has reported that noble metals supported on La-based oxides [4] are very stable and have low carbon formation at 550 °C in a MR built using a commercial self-standing Pd membrane [6]. For Rh [6] and Ru/La_2O_3 [7] formulations, the strong metal-support interaction is responsible for their high stability. The membrane plays a key role in the MR performance. This is why at present there is an intensive search for synthesizing composite membranes due to the need to achieve high permeation fluxes, maintaining high H_2 selectivities and reducing costs. The support materials are required to have good mechanical and thermal stabilities and must be produced at a reasonable cost [8]. Porous ceramic materials [9,10] and stainless steel [11,12] have been successfully used as substrates.

In the case of porous stainless steel (PSS) tubes, the size of the pore openings and roughness of the surface need to be conditioned in order to obtain thin defect-free Pd alloy membranes. In the last few years, several oxides such as Al_2O_3 [13,14] and ZrO_2 [15] have been used as surface conditioners. Moreover, these oxides play the role of diffusion barriers to limit the migration of the components of the metallic support to the thin H_2 permeable layer.

In this study we selected NaA zeolite as a novel material to accomplish both objectives. The driving force behind the selection of this type of zeolite is that the synthesis can be carried out at 80 °C without template. The H_2 selective layer was made of either pure Pd or a Pd–Ag alloy. The test reaction was the dry reforming of methane using a well proven Rh/La_2O_3 catalyst [6].

* Corresponding author. Tel.: +54 342 4536861; fax: +54 342 4536861.
E-mail address: lmcornag@fiq.unl.edu.ar (L.M. Cornaglia).

0376-7388/$ – see front matter © 2010 Elsevier B.V. All rights reserved.
doi:10.1016/j.memsci.2010.07.039

2. Experimental

2.1. Stainless steel support

PSS supports (316 L) were purchased from Mott metallurgical corporation (0.2 μm grade, 6.4 mm i.d., 9.5 mm o.d.). Before deposition, one end of PSS was welded to a non-porous stainless steel tube and the other one to a non-porous SS plug. The supports were cleaned in an alkaline solution (NaOH, 74 g l^{-1}; $NaHCO_3$, 51 g l^{-1}; Na_2HPO_4, 17 g l^{-1}) for grease and dirt removed, based upon Guazzone et al. [16]. The cleaning was performed in an ultrasonic bath at 60 °C, followed by rinsing in deionized water and isopropanol [17]; then the supports were dried overnight at 120 °C. After cleaning, the supports were oxidized in stagnant air at 500 °C for 12 h.

2.2. Modified support

After oxidation, the surface of the porous metal supports was modified with NaA zeolite, employing two different methods: (i) hydrothermal synthesis (HS) with secondary growth for the palladium membrane and (ii) dip coating of NaA zeolite with intermediate short Pd depositions for the Pd–Ag membrane [18].

(i) The NaA-HS/PSS was prepared by hydrothermal synthesis with secondary growth. The seeding layer was coated on the outer surface of the oxidized support by the vacuum-assisted seeding method using an ejector water jet pump, which was used to generate a pressure difference between the two sides of the support walls [19]. The tube connected to a vacuum system was fixed vertically and twice immersed for 3 min in a cylindrical vessel containing a colloidal suspension. This suspension was prepared by dispersing 2 g of A-type zeolite seed in 10 ml of water in an ultrasonic bath at 40 °C, followed by a centrifugation step to obtain the final suspension.

In order to prepare the synthesis gel, two precursors (Na aluminate and silica) were mixed with vigorous stirring at the synthesis temperature (80 °C). The aluminate solution was prepared by dissolving 7.70 g of sodium hydroxide and 6.07 g of sodium aluminate in 120 ml deionized water at room temperature. The silica suspension was prepared by mixing 3.56 g of silica and 53.3 ml of deionized water. The seeded support was placed vertically in a container with the synthesis gel for 8 h, and vacuum was applied. The inner and outer parts of the support were washed with deionized water, and then dried at 80 °C overnight [19]. One hydrothermal synthesis was performed.

(ii) The NaA-Pd/PSS was synthesized by dip coating of the NaA zeolite with intermediate short Pd depositions. Two different slurries (A and B) were prepared with NaA zeolite. Slurry A was prepared by dispersing 1 g of NaA zeolite in 80 ml of water. Slurry B was obtained by dispersing of 0.2 g in 80 ml of water.

During the dip coating of the NaA zeolite, the oxidized porous stainless steel tube was connected to a vacuum system. The first step involved immersion for 1 min in a cylindrical vessel containing colloidal slurry A in an ultrasonic bath followed by rinsing. This process was repeated with the same suspension during 5 min followed by Pd electroless plating for 5–10 min at 50 °C, without vacuum. Then, the last immersion was carried out with slurry B followed by a short Pd deposition. The modified support was rinsed and dried at 120 °C overnight.

2.3. Metallic deposition

The modified substrates were activated by the conventional two-step $SnCl_2/PdCl_2$ procedure [17]. This sequence was repeated between three and six times to obtain the activation layer. The solution concentrations were 1 g l^{-1} of $SnCl_2{\cdot}2H_2O$ (pH = 2) and 0.1 g l^{-1} of $PdCl_2$ (pH = 2) [17]. Electroless plating (ELP) was used to coat the PSS with a continuous metallic layer. The electroless plating compositions are summarized in Table 1. When the membrane was impermeable to liquid the plating was carried out with vacuum in order to block the last remaining large pores [18]. The activation-plating procedure was repeated until the composite membrane became impermeable to N_2 at room temperature and at a pressure difference of 10 kPa. The lowest flux that can be detected by our bubble flow meter is $\sim 4 \times 10^{-5}$ mol m^{-2} s^{-1}. The film thickness was estimated from the weight gain after metal deposition and checked by SEM. The membranes were heated in flowing nitrogen at 0.5 °C min^{-1} up to the desired temperature. The synthesized membranes are summarized in Table 2.

Table 1
Composition of Pd and Ag plating solutions.

	Pd bath	Ag bath
$PdCl_2$ (g l^{-1})	3.6	4.9
Na_2EDTA (g l^{-1})	67	33.6
NH_4OH (28%) (ml l^{-1})	650	650
HCl (37%) (ml l^{-1})	5	–
N_2H_4 (1 M) (ml l^{-1})	10	10
pH	~11	~11
Temperature (°C)	50	45

The Pd–Ag membrane was annealed at 500 °C during 220 h in H_2 atmosphere. The Pd membrane was activated in the same atmosphere for 65 h, at 350 °C. A pressure difference of 10 kPa was applied during the annealing and/or activation steps.

2.4. Gas permeation measurements

The membranes were evaluated in pure gases before use. Thermal treatments and gas permeation measurements were conducted in a shell-and-tube membrane module. The open end of the membrane was sealed to the permeator wall with Teflon ferrules. The permeator was placed in an electrical furnace and heated to the desired temperatures. A thermocouple within the membrane tube monitored and controlled the temperature during the experiments. All the gases were fed to the permeator using calibrated mass-flow controllers. Feed gases flowed along the outside of the membrane while the permeated gases flow rates were measured in the inner side of the membrane. A N_2 sweep gas stream was fed in the permeate side only during the heating and cooling periods. Pressure differences across the membranes were controlled using a back-pressure regulator. The upstream was varied while keeping the downstream pressure constant at 101.3 kPa. The gas permeation flow rates of either H_2 or N_2 were measured using two bubble flow meters at room temperature and pressure. A hydrogen purity of ~99.92% is the highest limit of accuracy estimated with this method.

2.5. Membrane reactor

Both membranes were used in a membrane reactor for the dry reforming of methane at 450 and 500 °C. The Rh/La_2O_3 catalyst was prepared by the conventional wet impregnation of $RhCl_3{\cdot}3H_2O$ onto La_2O_3 (Alfa) with a Rh loading of 0.6 wt.%. The impregnated solid was then heated at 80 °C to evaporate the water, and dried at 110 °C overnight. The catalyst was calcined for 6 h at 550 °C in flowing air.

The double tubular membrane reactor (Fig. 1) was built using the Pd or the Pd–Ag composite membranes (inner tube) mentioned above. The catalyst (2.4 g, p.d. = 0.15 mm), diluted with quartz chips (1.6 g—100 mesh), to achieve a bed height of 3 cm, was packed in the outer annular region (shell side). The outer tube was made of

Table 2
Pd–Ag membranes summary.

Membrane	Method	Thermal treatment		Thickness (μm)
		Temperature (°C)	Time (h)	
PdAg/NaA-Pd/PSS	Dip coating	500	220	23
Pd/ NaA-HS/PSS	Hydrothermal synthesis	350	65	20

commercial non-porous quartz (i.d. 16 mm). The inner side of the membranes in all runs was kept at atmospheric pressure. The catalysts were heated in Ar at 450 °C and then reduced in situ in H_2 at the same temperature for 3 h. After reduction, the temperature was adjusted in flowing Ar to the reaction temperature; and the feed stream gas mixture (33 vol.% CH_4, 33 vol.% CO_2, 34 vol.% Ar, $W/F = 2.4 \times 10^{-3}$ g h ml^{-1}, $P = 101.3$ kPa) was then switched to the reactor. Ar was employed as sweep gas. The feed gases and the reaction products were analyzed with two on-line thermal conductivity detector gas chromatographs: a Shimadzu GC-8A and a SRI 8610C (SRI Instruments (USA)). The former instrument was equipped with a Porapak column, and the latter with a molecular sieve column.

2.6. X-ray diffraction

The XRD patterns of the films were obtained with an XD-D1 Shimadzu instrument, using Cu Kα radiation at 30 kV and 40 mA. The scan rate was 1–2° min^{-1} in the range $2\theta = 30$–100°.

2.7. Scanning electron microscopy, energy-dispersive X-ray analysis

The outer surface and cross-section images were obtained using a JEOL scanning electron microscope, model JSM-35C, equipped with an energy-dispersive analytical system (EDAX). For the cross-section views, tubular pieces with a length of ~12 mm were placed in a plastic tube; then epoxy resin was added. After hardening, they were cut. The grinding was carried out with waterproof abrasive paper of 180, 280, 500, 800 and 1200 grit. The polishing was done with a ~1 μm grade paste, and finally with a suspension of γ-alumina (50 nm). The grinding and the polishing cycles lasted 5 min; after each cycle, it was necessary to clean the samples with ethyl alcohol in an ultrasonic bath. The final rinsing was performed with isopropanol.

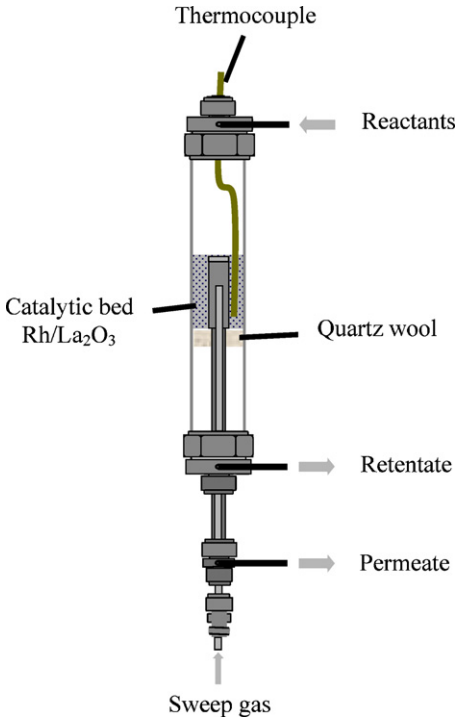


Fig. 1. The membrane reactor scheme.

2.8. X-ray photoelectron spectroscopy

XPS analyses were performed in a multi-technique system (SPECS) equipped with a dual Mg/Al X-ray source and a hemispherical PHOIBOS 150 analyzer operating in the fixed analyzer transmission (FAT) mode. The spectra were obtained with a Mg Kα X-ray source (100 W and 10 kV) or a monochromated Al Kα X-ray source (300 W and 12 kV). The working pressure in the analyzing chamber was less than 5×10^{-10} kPa. The XPS analyses were performed on the modified support and on the used membranes after being exposed to ambient conditions. The membranes were heated up in flowing H_2/Ar at 400 °C, and the modified substrates were heated up in vacuum at 300 °C in the reaction chamber of the spectrometer. The spectral region of Pd 3d, Pd 3p, Ag 3d, O 1s, C 1s, Si 2p, Na 1s, Fe 2p, Cr 2p and Al 2p were recorded for each sample. The data treatment was performed with the Casa XPS program (Casa Software Ltd., UK). The peak areas were determined by integration employing a Shirley-type background. Peaks were considered to be a mixture of Gaussian and Lorentzian functions in a 70/30 ratio. For the quantification of the elements, sensitivity factors provided by the manufacturer were used.

3. Results and discussion

3.1. H_2 permeation measurements

The hydrogen permeation measurements were carried out for the Pd/NaA-HS/PSS and PdAg/NaA-Pd/PSS membranes. The support, for the palladium membrane, was modified by hydrothermal synthesis and for the Pd–Ag membrane, the support was conditioned by dip coating. The thermal cycles applied to the membranes during the hydrogen and nitrogen measurements are shown in Fig. 2. The pressure difference was varied between 10 and 100 kPa. No nitrogen flow was observed at low pressure (<40 kPa) in any cycle. After the measurements, the ΔP was maintained at 10 kPa, in H_2 atmosphere.

Both membranes were evaluated at 400, 425 and 450 °C feeding pure gases. The H_2 flow and the ideal selectivities are shown in Figs. 3 and 4. The ideal selectivity is defined as the ratio between the fluxes of the two pure gases (H_2 and N_2), under the same transmembrane pressure difference and temperature. On the other hand, the hydrogen flux shows a linear dependence on $\left(P^n_{H_2,\,\mathrm{ret}} - P^n_{H_2,\,\mathrm{perm}}\right)$ and an increase with temperature. The best fit was obtained with $n = 0.5$ with a regression coefficient around 0.99992. This behavior is characteristic of the hydrogen transport through a dense Pd-based alloy membrane, known as the solution-diffusion mechanism (Sievert's law). However, in order to confirm the n-value, it would be interesting to apply higher pressure intervals [20].

The supports offered a low resistance for the hydrogen transport. In all cases the calculated pressure drop was lower than 9 kPa for a ΔP applied equal to 100 kPa. The pressure drop was estimated

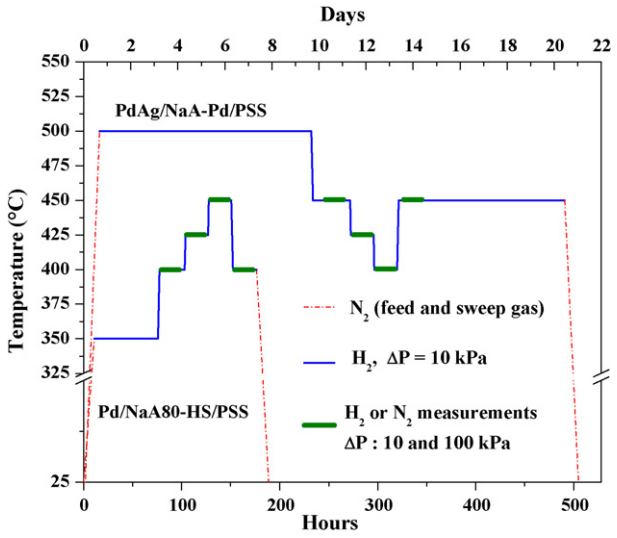


Fig. 2. The effect of pressure on the permeate hydrogen flux.

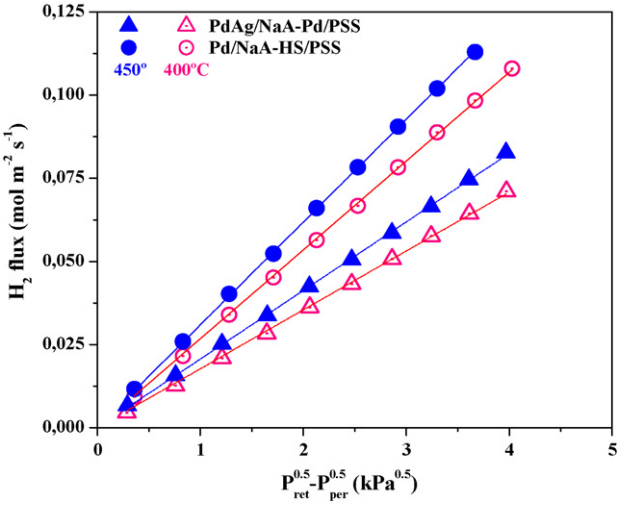


Fig. 3. Effect of transmembrane pressure difference upon ideal selectivity.

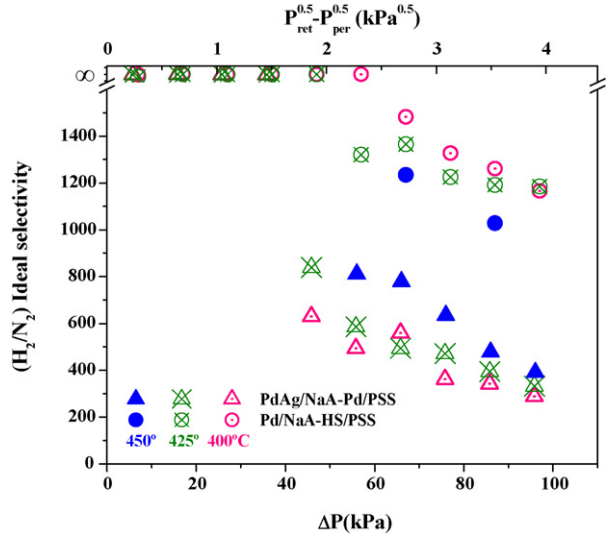


Fig. 4. Thermal cycles.

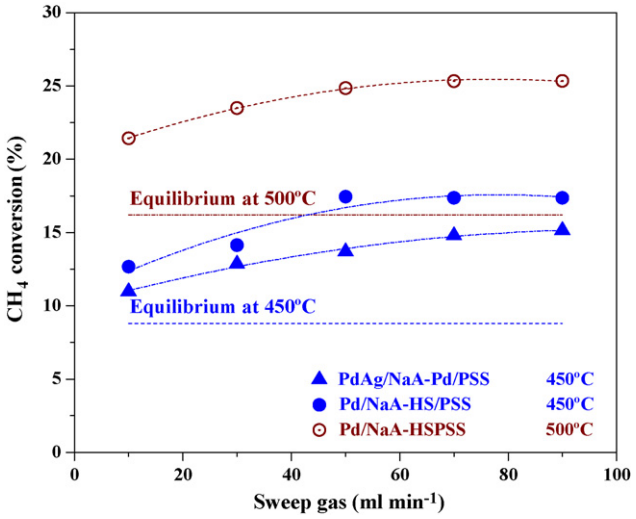


Fig. 5. Variation of the methane conversion for the dry reforming reaction with the sweep gas. Rh (0.6%)/La_2O_3 ($W/F = 2.4 \times 10^{-3}$ g h ml^{-1}), reactant gas mixture CH_4:CO_2:Ar (1:1:1.1), P = 101.3 kPa, permeation area = 7.3 cm^2.

considering the composite membrane (the metallic layer and modified support) as series resistances. Knudsen and viscous fluxes occur through the porous support and defects of the metallic film.

The ideal selectivities decreased with the increase of the applied pressure difference. This behavior can be explained taking into account the possible permeation mechanisms. As mentioned in the previous paragraph, hydrogen permeates mainly by the solution-diffusion mechanism and nitrogen permeates through pinholes of the film. The nitrogen flux is controlled by Knudsen and viscous mechanisms that present a linear dependence on ΔP.

For the Pd/NaA-HS/PSS membrane, a slight selectivity decrease with temperature was observed, probably due to the pinhole formation during the temperature cycling performed in the long-term operation. However, the Pd membrane showed a higher efficiency for hydrogen separation, reaching selectivities above 1000 (99.90% hydrogen purity), even at ΔP = 100 kPa. Besides, this membrane shows the highest H_2 flux in the applied pressure range.

The permeation data will be compared with other reports that also employed porous stainless steel support and electroless plating for metallic deposition. The H_2 permeance at 450 °C, considering Sievert's law, was equal to 9.71×10^{-4} mol m^{-2} s^{-1} Pa$^{-0.5}$ for the Pd/NaA-SH/PSS membrane (20 μm). This value is higher than the one reported by Samingprai et al. [21] for a Pd membrane of 32 μm (5.19×10^{-5} mol m^{-2} s^{-1} Pa$^{-0.5}$ at 450 °C). They modified the porous support (316 L, grade 0.1 μm) with chromium oxide deposition by electroplating. On the other hand, Zhang et al. [22] showed a similar H_2 permeance (7.4×10^{-4} mol m^{-2} s^{-1} Pa$^{-0.5}$ at 500 °C) for a membrane supported on 316 L (grade 0.5 μm) with a thickness of 11 μm. The support was modified with sol–gel derived mesoporous yttria stabilized zirconia.

3.2. Membrane reactor

Fig. 5 shows the methane conversions for both membranes. The values of the thermodynamic equilibrium conversions at 450 and 500 °C are also shown. They were calculated considering the simultaneous occurrence of both reactions, dry reforming and reverse water gas shift.

Due to its better performance, the Pd/NaA-HS/PSS membrane was also evaluated at 500 °C. As expected, conversion increased with the sweep gas flow rate. The increase in CH_4 conversion for the Pd membrane was 97% and 53% with respect to the equilibrium conversions at 450 and 500 °C, respectively. In all cases the carbon

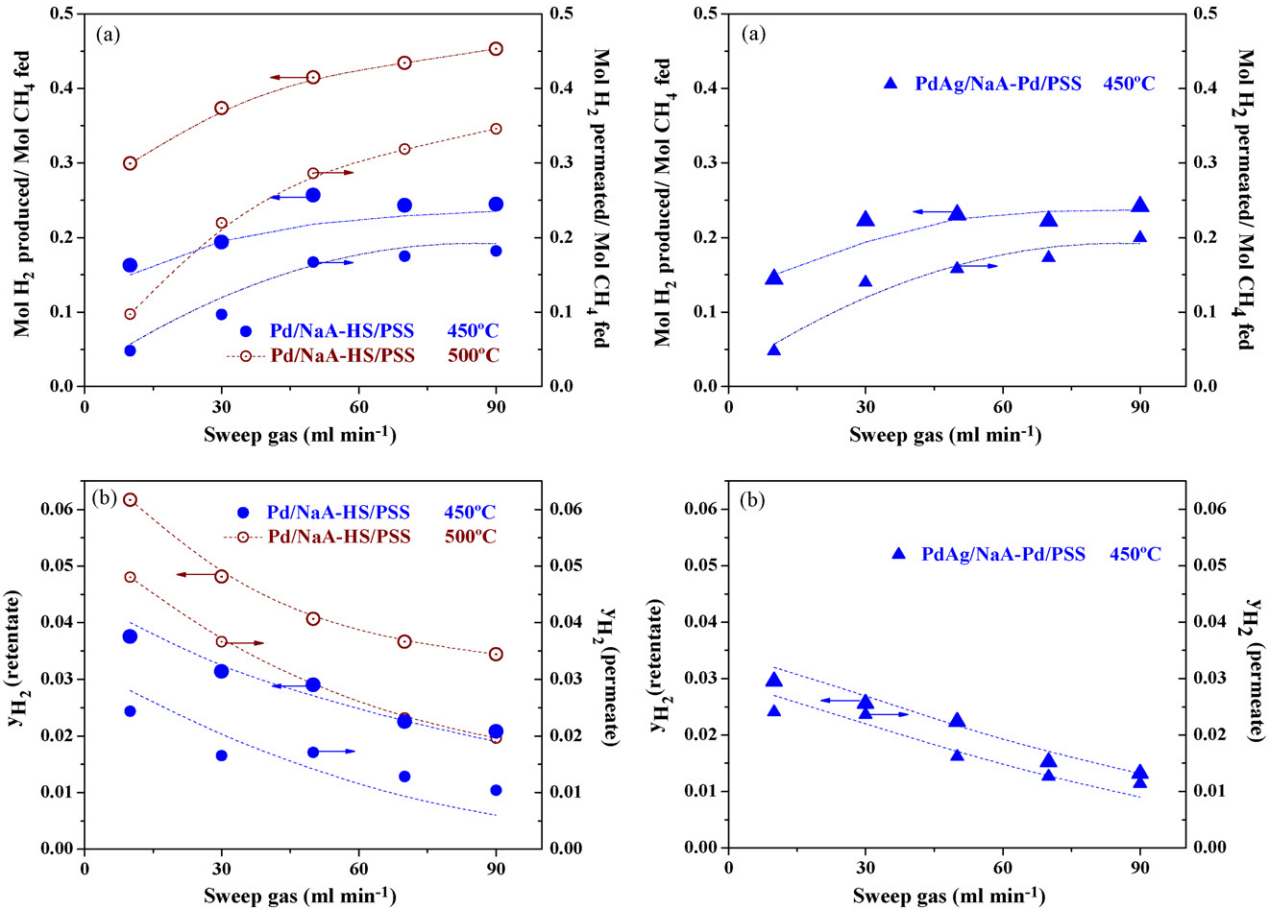


Fig. 6. Comparison of the effect of the sweep gas upon the permeated hydrogen flow. Rh (0.6%)/La_2O_3 ($W/F = 2.4 \times 10^{-3}$ g h ml^{-1}), reactant gas mixture CH_4:CO_2:Ar (1:1:1.1), P = 101.3 kPa, permeation area = 7.3 cm^2.

balance was higher than 98.5%, indicating that no coke deposition occurred.

The permeated hydrogen flow per mol of CH_4 fed increases with the sweep gas flow rate (Fig. 6a). On the other hand, this ratio shows a significant increase with the reaction temperature (Fig. 6a), reaching a value of 0.35 at 500 °C and maximum sweep gas flow rate for the Pd membrane. The Pd and PdAg membranes exhibit a similar increase with the sweep gas flow rate for both H_2 ratios at 450 °C (Fig. 6a). However, the hydrogen (Fig. 6b) and CO (not shown) molar fractions in the retentate side are higher for the Pd membrane. A possible reason for this H_2/CH_4 behavior could be the high CO concentration that decreases the hydrogen flow of the Pd membrane, thus blocking the active sites for the hydrogen dissociation.

Moreover, the permeate selectivities (H_2/CH_4) observed during the reaction (Fig. 7) are higher for the Pd/NaA-HS/PSS membrane. Also note that, the H_2/CH_4 ratios increase with increasing sweep gas flow rate (ΔP). These results suggest that at low sweep gas flow rates the hydrogen permeation is low. Mejdell et al. [20] have discussed the influence of several effects on hydrogen permeation when hydrogen is present in a gas mixture: (i) competitive adsorption of other gas components that reduces the fraction of sites available for hydrogen adsorption and dissociation, (ii) the bulk gas depletion along the retentate side due to selective removal of hydrogen, and (iii) the concentration polarization due to gas phase mass transport limitations.

During the water gas shift (WGS) reaction carried out in a membrane reactor, Arstad et al. [23] observed a reduction in the hydrogen flow rate through the membrane. For this reason they studied the effect of CO on hydrogen permeation during the reactions of WGS and methanol steam reforming. In WGS experiments, they found a slow accumulation of strongly adsorbed species, although not irreversible, that blocked the hydrogen adsorption/dissociation process. In contrast, the concentration of CO in the reforming of methanol was low; in this case the permeation was limited by adsorbed species from unconverted methanol. However,

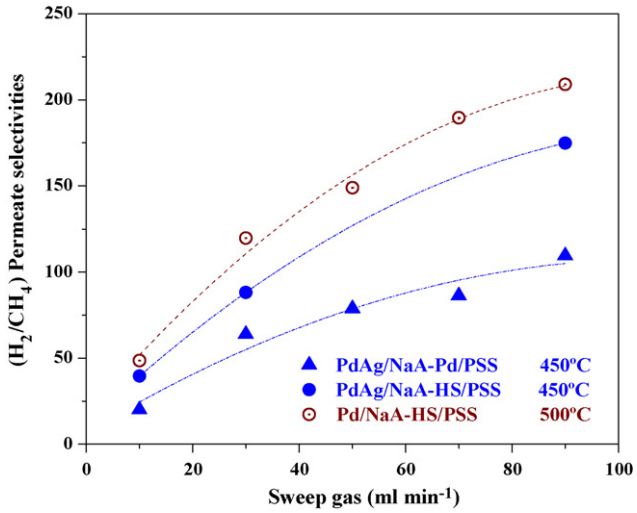


Fig. 7. Permeation selectivity (H_2/CH_4) versus sweep gas. Rh(0.6%)/La_2O_3 ($W/F = 2.4 \times 10^{-3}$ g h ml^{-1}), reactant gas mixture CH_4:CO_2:Ar (1:1:1.1), P = 101.3 kPa, permeation area = 7.3 cm^2.

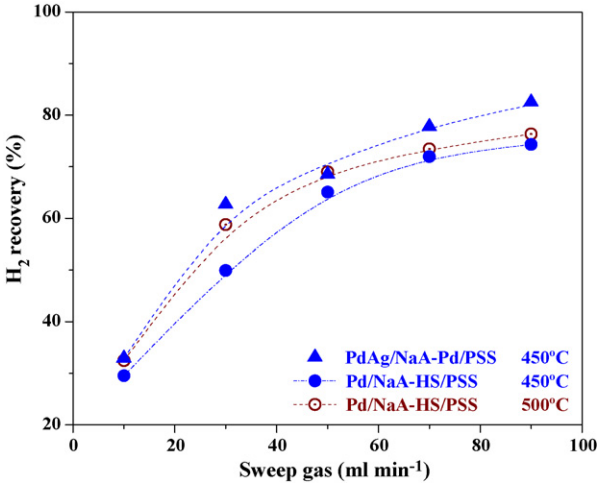


Fig. 8. Effect of sweep gas on H_2 recovery. Rh (0.6%)/La_2O_3 ($W/F = 2.4 \times 10^{-3}$ g h ml^{-1}), reactant gas mixture CH_4:CO_2:Ar (1:1:1.1), P = 101.3 kPa, permeation area = 7.3 cm^2.

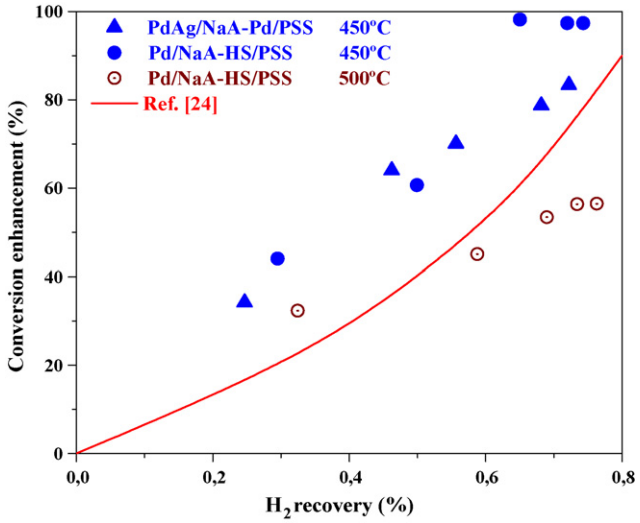


Fig. 9. Correlation between the methane conversion enhancement and the H_2 recovery. Rh (0.6%)/La_2O_3 ($W/F = 2.4 \times 10^{-3}$ g h ml^{-1}), reactant gas mixture CH_4:CO_2:Ar (1:1:1.1), P = 101.3 kPa, permeation area = 7.3 cm^2.

at high concentrations of hydrogen, the methoxy groups could be hydrogenated to methanol and then they are desorbed liberating adsorption/dissociation sites [23]. In our case, the increase on selectivity with the sweep gas flow rate is probably due to the coverage of the metal surface by reaction gases inhibiting the dissociation of H_2.

Oyama and Lim [24] performed the numerical simulation of a membrane reactor and they found that membranes with H_2/CH_4 selectivities of 100 showed essentially the same enhancement of both the methane conversion and H_2 yield as the membrane with infinite hydrogen selectivity. This comparison was carried out at constant hydrogen permeance. They concluded that H_2/CH_4 permeate selectivities greater than 100 allow high yield in the MRs. Our palladium membrane, exhibited the highest H_2/CH_4 selectivity (200), which was observed at 90 ml min^{-1} (sweep gas) and 500 °C (Fig. 7), with a permeate hydrogen purity equal to 99.5%. This value exceeds the highest value corresponding to the PdAg/NaA-Pd/PSS membrane, equal to 98.7% (at 90 ml min^{-1}).

Another key parameter for membrane reactors is the percentage recovery of hydrogen defined as the ratio of the H_2 permeated and the H_2 produced. Fig. 8 shows that the PdAg/NaA-Pd/PSS membrane exhibited 83% hydrogen recovery for a sweep gas flow rate of 90 ml min^{-1}, with a selectivity (H_2/CH_4) equal to 105. However, the Pd/NaA-HS/PSS membrane showed the best performance in the membrane reactor for the dry reforming reaction. When the MR was operated at 500 °C, the H_2 recovery reached ~72% (Fig. 8) and the H_2/CH_4 selectivity was equal to 200 (Fig. 7). Bearing in mind the significant increase in conversion and permeate flow, and that both the selectivity and H_2 recovery remained constant over time (24 h) at 500 °C, these conditions are promising for Pd membrane application in membrane reactors.

According to the DOE (Department of Energy U.S.) H_2 program, one of the targets in membrane reactors is to reach a hydrogen recovery of 80% and a hydrogen purity of 99.5% for the year 2010 [25,26]. Our PdAg/NaA-Pd/PSS membrane showed a value close to 80% hydrogen recovery (Fig. 8) when the sweep gas flow rate was 90 ml min^{-1}. The Pd/NaA-HS/PSS produced hydrogen with 99.5% of purity, this value was calculated considering only H_2 and the permeated gases.

In our case, the composite membranes were treated in H_2 flux and then the permeation measurements were performed. Afterwards, they were cooled down to room temperature and then used in the membrane reactor. After these treatments, both membranes were thermally stable up to 450 °C; the pure Pd membrane maintained constant its permselective properties during at least 250 h while the Pd–Ag system was did so during 570 h. After the reaction tests at high sweep gas flow rates and temperatures, the sweep gas flow was decreased up to 10 ml min^{-1}, and then the hydrogen flow and methane conversion were measured. These values remained unchanged in comparison with the initial ones.

Oyama and Lim [24] calculated the methane conversion enhancement in function of the "operability level coefficient" (OLC) through a one-dimensional mathematical simulation developed to describe the performance of the methane steam-reforming reaction at 500 °C in a MR. This temperature was chosen by the authors because it was in the middle of the temperature range used in the reforming reactions [24]. The OLC parameter was defined as the ratio of the actual permeation rate and the actual formation rate of a critical product in a membrane reactor, where the critical product is the one for which the membrane is permselective [24]. They found a clear universal trend for increasing conversions with increasing OLC for different types of reforming reactions.

Fig. 9 presents the percent methane conversion enhancement as a function of the hydrogen recovery for our membranes (note the equivalence between the OL coefficient and the H_2 recovery). These values were calculated for several sweep gas flow rates, and they follow the same tendency shown by the solid line (curve obtained from Oyama and Lim [24]).

3.3. Characterization

3.3.1. Modified supports

After oxidation, the supports were conditioned with NaA zeolite. Fig. 10 shows the XRD patterns of the modified supports. The diffractogram obtained after the hydrothermal synthesis (Fig. 10a) displays only the diffraction features of the γ-phase (austenite) at 43°, 50.2°, 74°, 90.1° and 95.3° [19,27], suggesting that the zeolitic material was mainly deposited in the internal pore system. The diffractogram obtained after the vacuum-assisted dip coating and short Pd depositions (Fig. 10b) shows the reflection peaks of both the γ-phase (austenite) and pure palladium (at 39.6°, 46.2°, 67.6°, 81.7° and 86°), suggesting that the metallic deposition is <1 μm thick [28].

The morphologic features of the modified support were examined by SEM. The top (a–d) and cross-sectional (e–f) views with different magnifications are shown in Fig. 11. The top views for

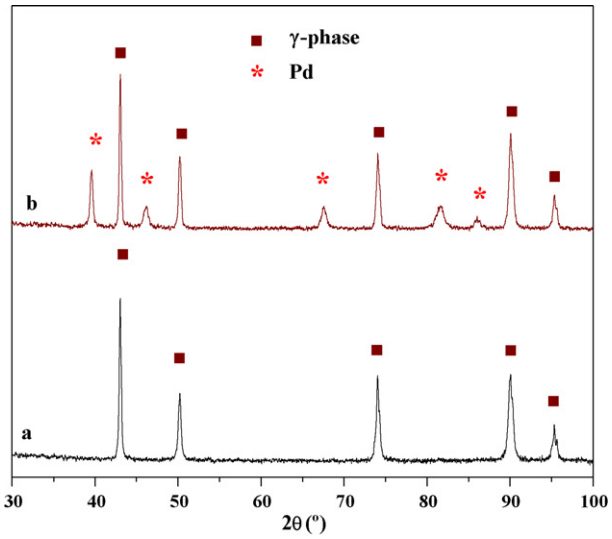


Fig. 10. Diffractograms of (a) NaA-HS/PSS and (b) NaA-Pd/PSS.

Table 3
Atomic surface concentrations determined by EDS.

Point	Pd	Fe	Si	Al
a.1	97.45	2.55	–	–
a.2	–	–	10.09	10.24

The remaining percentage corresponds to Cr, Ni, Mo and Na.

NaA-HS/PSS (Fig. 11a and b) show typical aggregates of cubic NaA zeolite crystals [19] with sizes between 1 and 3 μm. An incomplete intergrowth among these aggregates is observed. Several edges, corners and ridges of individual crystals are evident. The NaA cubic crystals can also be observed in the internal pore system (Fig. 11e). The top views of NaA-Pd/PSS show non-uniform morphology. The cross-section views of the modified supports (Fig. 11e and f) show the penetration of the modifier into the pore system, without the formation of a continuous external layer (Fig. 12).

The elemental analyses at volumetric level, were performed by EDS (Table 3). A high concentration of Pd at the external surface can be observed in point a.1. On the other hand, on a zeolite crystal (point a.2), the Si and Al contents are similar, in agreement with the NaA chemical formula.

The elemental analyses at surface level were performed by XPS. The XPS data (Table 4) show similar surface atomic concentrations of Si and Al for each modified support. Pd was detected on the mod-

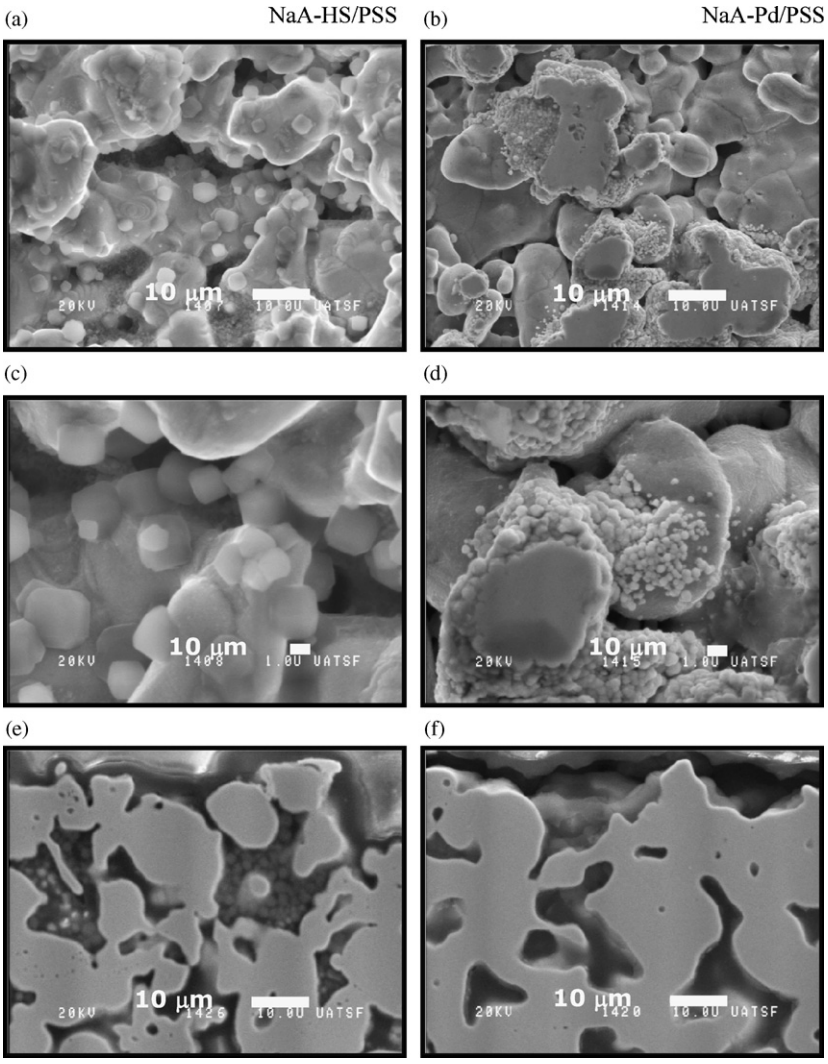


Fig. 11. SEM images of the modified supports. Top views (a–d) and cross-sectional views (e–f) at different magnifications (600×, 1800×).

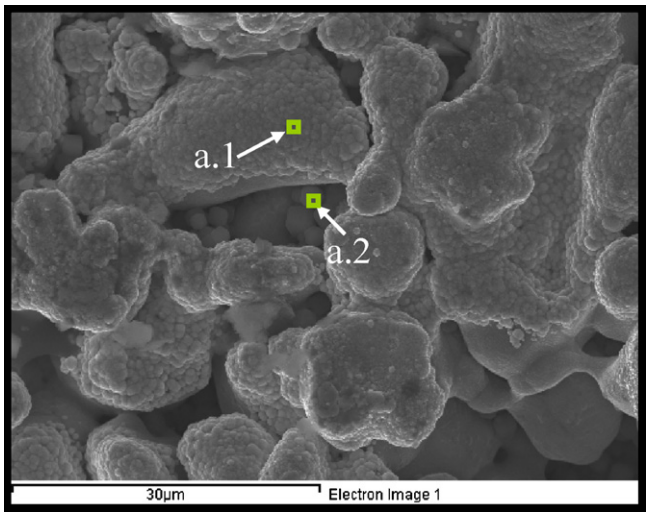


Fig. 12. EDS analysis of the NaA-Pd/PSS support.

Table 4
Atomic surface concentrations on modified and oxidized supports determined by XPS.

Sample	Cr (%)	Fe (%)	Pd (%)	Si (%)	Al (%)
Oxidized PSS	11.26	88.74	–[a]	–[b]	–[a]
NaA-HS/PSS	8.25	34.43	–[a]	27.60	29.71
NaA-Pd/PSS	5.27	10.95	42.65	21.60	19.52

[a] Pd or Al are not detected.
[b] Not measured.

ified support surface of NaA-Pd/PSS. On the other hand, both Fe and Cr atomic concentrations were lower than the values of the NaA-HS/PSS support, due to the presence of Pd.

3.3.2. Composite membranes

The diffractograms of the Pd–Ag membrane are shown in Fig. 13. The disappearance of Ag reflections and the presence of new peaks corresponding to the Pd–Ag alloy are observed after annealing in a H_2 reducing atmosphere at 500 °C. However, low intensity Pd peaks are still detected, suggesting that the alloy formation was not complete [29]. The diffractogram obtained after the dry reforming of methane (Fig. 13b) shows a slight separation between the reflection peaks of the alloy and pure palladium; however, the relative intensities between the peaks remain constant. This diffractogram is similar to that obtained before the reaction measurements (Fig. 13a), indicating that the reaction conditions employed (temperature and reactant composition) did not affect the crystalline structure of the Pd–Ag membrane. The X-ray diffraction patterns of the Pd/NaA-HS/PSS membrane are not shown because they only present the pure palladium peaks.

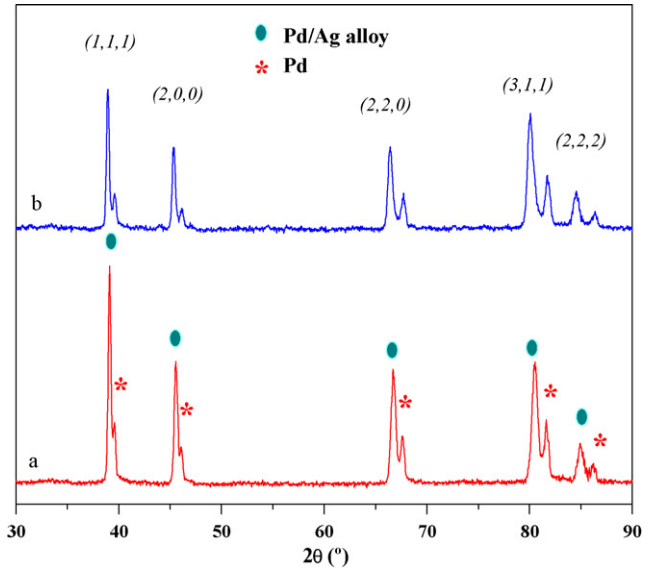


Fig. 13. XRD pattern of the PdAg/NaA-Pd/PSS membrane. (a) After annealing at 500 °C in H_2 atmosphere and (b) after reaction at 450 °C.

Table 5
Concentrations measured on the pores of the support and the metallic film of the PdAg/NaA-Pd/PSS membrane from EDS.

Point	Pd	Ag	Al	Si	Fe[a]
b.0	78	22	–	–	–
b.1	66	–	5	2	19
b.2	2	–	24	20	37
b.3	5	–	29	31	25
b.4	2	–	32	43	16

[a] The remaining percentage corresponds to Cr, Ni and Mo.

Fig. 14 shows the SEM micrographs of the cross-section and top views of the Pd–Ag membrane after use in the membrane reactor. The top view (Fig. 14a) shows the characteristic morphology of the Pd–Ag film synthesized by electroless plating with well-defined boundaries [28]. This membrane has a large amount of small clusters (5–10 µm) of rounded shape, which grew over other bigger ones. The small pores observed in the metallic film (Fig. 14b) could be related to the dendritic and non-uniform silver deposits, whose growth is preferentially perpendicular to the substrate surface [12,30]. The Pd–Ag penetrated into the pore system and the resulting layer showed thicknesses that were at some areas (inside the pores) larger than the one determined by the gravimetric method equal to 23 µm. These thicknesses were between 16 and 32 µm.

The elemental composition of the metal film and the substrate was determined by EDS; Fig. 14 shows the measured regions. The Ag average elemental composition, measured on-line b on the film, was 11%. The Ag composition was not homogeneous across the film thickness, suggesting that the alloy has not been completely formed, in agreement with the XRD data (Fig. 13).

Note that there is Ag enrichment on the outer surface where the concentration is ~22% (Fig. 14). For the Pd–Ag membrane, the elemental composition of several points (b.1, b.2, b.3 and b.4) located inside the modified porous support (Fig. 14) are summarized in Table 5.

Two points (b.2 and b.3) (Fig. 14) have Si and Al with similar concentrations, this was expected because the ratio of Si/Al is unity in the NaA zeolite. Moreover, the Pd has a high concentration only in a pore near the outer surface of the substrate (b.1). Therefore, this substrate modification allowed the Pd to enter only into in the external pores, while Al and Si penetrated up to 40 µm. This would provide anchoring sites [18] for the Pd layer, increasing the adhesion between the metal film and the porous stainless steel.

To study the metal surface segregation, the PdAg/NaA-Pd/PSS membrane after annealing at 500 °C, permeation and reaction measurements was characterized by XPS. The peak positions of the Ag $3d_{5/2}$ and Pd $3d_{5/2}$ core-levels were observed at 334.9 ± 0.1 and 367.5 ± 0.1 eV, respectively (Table 6). The binding energy of Ag $3d_{5/2}$ level is lower than that corresponding to pure silver (Table 6). The BE shift is consistent with the one reported for Pd–Ag alloys [32] and suggests formation of the surface alloy.

Ag surface concentration was higher than the value determined by EDS, being equal to 46.3%. The Ag surface segregation can be associated with the surface tension difference between of the pure metals [33].

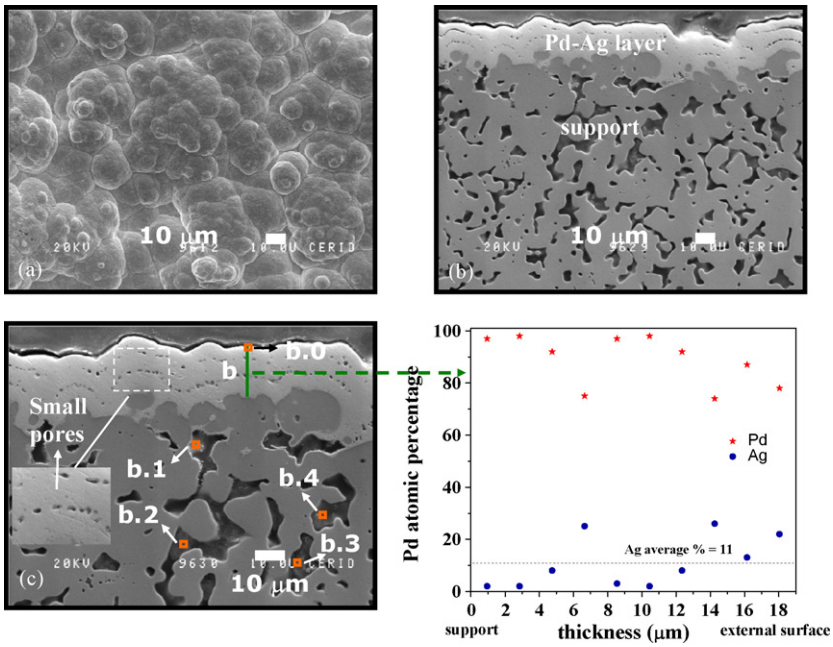


Fig. 14. SEM images and EDS data of the Pd–Ag/NaA-Pd/PSS membrane. (a) Top view, (b) cross-section view and (c) EDS measured regions.

Table 6
Pd 3d and Ag 3d XPS binding energies and relative concentrations.

Membrane	Ag $3d_{5/2}$ (eV)	Pd $3d_{5/2}$ (eV)	Ag % XPS	Ag % EDS[a]
PdAg/NaA-Pd/PSS	367.5	334.9	46.3	27
Pure Ag[b]	368.3	–	–	–
Pure Pd[c]	–	335.4	–	–

[a] Value measure in a top view of the membrane with a magnification of 60×.
[b] Measured in our instrument.
[c] Ref. [31].

4. Conclusions

The NaA zeolite was a good choice as a support modifier. The zeolite basically penetrates into the pore system (up to 40 μm) of the stainless steel substrate. This structure facilitates the deposition of a thin continuous metallic layer. The Pd membrane showed a high efficiency for hydrogen separation, reaching selectivities above 1000, even at $\Delta P = 100$ kPa.

The composite membranes are thermally stable up to 450 °C; the pure Pd membrane was stable for at least 250 h while the Pd–Ag system was stable for 570 h. After reaction, neither the crystalline structure nor the morphological features of the composite membranes were modified.

Both membranes showed a good performance. The methane conversion enhancement of the dry reforming reaction was higher than 80% at 450 °C. At 500 °C the Pd/NaA-HS/PSS membrane showed the best behavior with a mol H_2 permeated/ mol CH_4 fed ratio of 0.35 and a hydrogen purity of 99.5%.

Acknowledgements

The authors wish to acknowledge the financial support received from UNL, CONICET an ANPCyT. They are also grateful to the Japan International Cooperation Agency (JICA) for the donation of the XRD and to ANPCyT for Grant PME 8-2003 to finance the purchase of the UHV Multi Analysis System. Thanks are also given to Prof. Elsa Grimaldi for the English language editing and to Fabio Fontanarrosa from CCT CONICET-SANTA FE for the SEM-EDS analyses.

References

[1] G.Q. Lu, J.C. Diniz da Costa, M. Duke, S. Giessler, R. Socolow, R.H. Williams, T. Kreutz, Inorganic membranes for hydrogen production and purification: a critical review and perspective, J. Colloid Interface Sci. 314 (2007) 589–603.
[2] E. Kikuchi, Y. Chen, Low-temperature syngas formation by CO_2 reforming of methane in a hydrogen-permselective membrane reactor, Stud. Surf. Sci. Catal. 107 (1997) 547–553.
[3] P. Ferreira-Aparicio, M. Benito, S. Menad, Catalysis in membrane reformers: a high-performance catalytic system for hydrogen production from methane, J. Catal. 231 (2005) 331–343.
[4] J.F. Múnera, L. Coronel, B. Faroldi, C. Carrara, E.A. Lombardo, L.M. Cornaglia, Production of ultrapure hydrogen in a Pd–Ag membrane reactor using noble metal supported on La-based oxides. Modeling for the dry reforming of methane reaction, Asia-Pac. J. Chem. Eng. 5 (2010) 35–47.
[5] D. Lee, P. Hacarlioglu, S.T. Oyama, The effect of pressure in membrane reactors: trade-off in permeability and equilibrium conversion in the catalytic reforming of CH_4 with CO_2 at high pressure, Top. Catal. 29 (2004) 45–57.
[6] S. Irusta, J. Múnera, C. Carrara, E.A. Lombardo, L.M. Cornaglia, A stable, novel catalyst improves hydrogen production in a membrane reactor, Appl. Catal. A 287 (2005) 147–158.
[7] B. Faroldi, C. Carrara, E.A. Lombardo, L.M. Cornaglia, Production of ultrapure hydrogen in a Pd–Ag membrane reactor using Ru/La_2O_3 catalysis, Appl. Catal. A 319 (2007) 38–46.
[8] S.-E. Nam, K.-H. Lee, Preparation and characterization of palladium alloy composite membranes with a diffusion barrier for hydrogen separation, Ind. Eng. Chem. Res. 44 (2005) 100–105.
[9] S.N. Paglieri, K.Y. Foo, J.D. Way, J.P. Collins, L. Harper-Nixon, A new preparation technique for Pd/Alumina membranes with enhanced high-temperature stability, Ind. Eng. Chem. Res. 38 (1999) 1925–1936.
[10] G. Zeng, A. Goldbach, H. Xu, Impact of support mass flow resistance on low-temperature H_2 permeation characteristics of a $Pd_{95}Ag_5/Al_2O_3$ composite membrane, J. Membr. Sci. 326 (2009) 681–687.
[11] C. Su, T. Jin, K. Kuraoka, Thin palladium film supported on SiO_2-modified porous stainless steel for a high-hydrogen-flux membrane, Ind. Eng. Chem. Res. 44 (2005) 3053–3058.
[12] R. Bhandari, Y.H. Ma, Pd–Ag membrane synthesis: the electroless and electroplating conditions and their effect on the deposits morphology, J. Membr. Sci. 334 (2009) 50–63.
[13] J. Tong, Y. Kashima, R. Shirai, H. Suda, Y. Matsumura, Thin defect-free Pd membrane deposited on asymmetric porous stainless steel substrate, Ind. Eng. Chem. Res. 44 (2005) 8025–8032.
[14] D. Yepes, L.M. Cornaglia, S. Irusta, E.A. Lombardo, Different oxides uses as diffusion barriers in composite hydrogen permeable membranes, J. Membr. Sci. 274 (2006) 92–101.
[15] Y. Huang, R. Dittmeyer, Preparation and characterization of composite palladium membranes on sinter-metal supports with a ceramic barrier against intermetallic diffusion, J. Membr. Sci. 282 (2006) 296–310.
[16] F. Guazzone, E.E. Engwall, Y.H. Ma, Effects of surface activity, defects and mass transfer on hydrogen permeance and n-value in composite palladium-porous stainless steel membranes, Catal. Today 118 (2006) 24–31.

[17] P.P. Mardilovich, Y. She, Y.H. Ma, M. Rei, Defect-free palladium membranes on porous stainless-steel support, AIChE J. 44 (1998) 310–322.
[18] F. Guazzone, Ph.D. Thesis in Chemical Engineering, Engineering of Substrate Surface for the Synthesis of Ultra-thin Composite Pd and Pd–Cu Membranes for H_2 Separation, Worcester Polytechnic Institute (2005).
[19] M.L. Bosko, F. Ojeda, E.A. Lombardo, L.M. Cornaglia, NaA zeolite as an effective diffusion barrier in composite Pd/PSS membranes, J. Membr. Sci. 331 (2009) 57–65.
[20] A.L. Mejdell, M. Jondahl, T.A. Peters, R. Bredesen, H.J. Venvik, Experimental investigation of a microchannel membrane configuration with a 1.4 μm Pd/Ag23 wt.% membrane—effects of flow and pressure, J. Membr. Sci. 327 (2009) 6–10.
[21] S. Samingprai, S. Tantayanon, Y.H. Ma, Chromium oxide intermetallic diffusion barrier for palladium membrane supported on porous stainless steel, J. Membr. Sci. 347 (2009) 8–16.
[22] K. Zhang, H. Gao, Z. Rui, P. Liu, Y. Li, Y.S. Lin, High-temperature stability of palladium membranes on porous metal supports with different intermediate layers, Ind. Eng. Chem. Res. 48 (2009) 1880–1886.
[23] B. Arstad, H. Venvik, H. Klette, J.C. Walmsley, W.M. Tucho, R. Holmestad, A. Holmen, R. Bredesen, Studies of self-supported 1.6 mm Pd/23 wt.% Ag membranes during and after hydrogen production in a catalytic membrane reactor, Catal. Today 118 (2006) 63–72.
[24] S.T. Oyama, H. Lim, An operability level coefficient (OLC) as a useful tool for correlating the performance of membrane reactors, Chem. Eng. J. 151 (2009) 351–358.
[25] U.S. Department of Energy, Office of Energy Efficiency and Renewable Energy, Table 3.1.7, April 2009.
[26] U.S. Department of Energy, Office of Fossil Energy, Table 9. Hydrogen Separation Technical Target, September 2009.
[27] C.J. Nuñez, M.V. Utrilla, A. Ureña, Effect of temperature on sintered austeno-ferritic stainless steel microstructure, J. Alloys Compd. 463 (2008) 552–558.
[28] M.E. Ayturk, E.E. Engwall, Y.H. Ma, Microstructure analysis of the intermetallic diffusion-induced alloy phases in composite Pd/Ag/porous stainless steel membranes, Ind. Eng. Chem. Res. 46 (2007) 4295–4306.
[29] M. Engin Ayturk, E.A. Payzant, S.A. Speakman, Y.H. Ma, Isothermal nucleation and growth kinetics of Pd/Ag alloy phase via in situ time-resolved high-temperature X-ray diffraction (HTXRD) analysis, J. Membr. Sci. 316 (2008) 97–111.
[30] J.N. Keuler, L. Lorenzen, R.D. Sanderson, V. Prozesky, W.J. Przybylowicz, Characterization of electroless plated palladium–silver alloy membranes, Thin Solid Films 347 (1999) 91–98.
[31] M. Brun, A. Berthet, J.C. Bertolini, XPS, AES and Auger parameter of Pd and PdO, J. Electron. Spectrosc. Relat. Phenom. 104 (1999) 55–60.
[32] P. Ptacek, Z. Bastl, XPS characterization of supported bimetallic palladium–silver clusters, Appl. Surf. Sci. 45 (1990) 319–323.
[33] J.B. Miller, C. Matranga, A.J. Gellman, Surface segregation in a polycrystalline Pd70Cu30 alloy hydrogen purification membrane, Surf. Sci. 602 (2008) 375–382.